Materials Advances

ROYAL SOCIETY OF CHEMISTRY

PAPER

View Article Online
View Journal | View Issue

Cite this: *Mater. Adv.*, 2021, **2**, 706

Conversion of conducting polypyrrole nanostructures to nitrogen-containing carbons and its impact on the adsorption of organic dye

Jaroslav Stejskal, *[a] Miroslav Kohl, [b] Miroslava Trchová, [c] Zdeňka Kolská, [d] Michal Pekárek, [a] Ivo Křivka [e] and Jan Prokeš [e]

New types of materials were produced by gradual heating of a conducting polymer, polypyrrole, to elevated temperatures. Three polymers differing in morphology – globules, nanofibers, and nanotubes – were exposed to temperatures from 100 to 700 °C in an argon atmosphere. The yields always exceeded 50 wt%, and the morphological features of the polymer were preserved. The transformation of polypyrrole salts to the corresponding bases followed by the carbonization was monitored by FTIR spectroscopy. The elemental analysis confirmed the subsequent conversion of polypyrrole to nitrogen-containing carbon. The specific surface areas were of the order of tens of $m^2\ g^{-1}$; they increased from globules to nanotubes and nanofibers but were virtually independent of the exposition temperature. The conductivity of the powders was compared with that of the pellets when their preparation was possible. As the temperature was increased up to 400 °C, the conductivity decreased for all samples by *ca.* 5 orders of magnitude, *e.g.*, for nanofibers from 10 to 10^{-4} S cm^{-1} but recovered to 10^{-1} S cm^{-1} after the subsequent carbonization up to 700 °C. Polypyrroles exposed to various temperatures were then tested for the adsorption of organic dye, Reactive Black 5, from water. The dye adsorption on original polypyrroles strongly depended on the polymer morphology. Polypyrrole nanofibers were able to remove the dye completely with a capacity of 100 mg g^{-1}, while the adsorption on polypyrrole globules was poor. The adsorption efficiency thus increased from globules to nanotubes and nanofibers. The adsorption performance was reduced after the carbonization, but the general trends were preserved.

Received 23rd September 2020,
Accepted 18th November 2020

DOI: 10.1039/d0ma00730g

rsc.li/materials-advances

1. Introduction

Conducting polymers, such as polyaniline and polypyrrole, have been of interest for a long time due to their electronic conductivity at the semiconductor level and the ease of their preparation.[1] The properties not directly associated with conductivity, such as electroactivity and responsivity to external stimuli, electrocatalytic activity, or polarizability, have recently come to the forefront.[2,3] The mixed contribution of electronic and ionic conductivity makes these polymers attractive for bio-applications.[4,5] The environmental issues presented by water-pollution treatment have also stimulated the generation of a vast amount of literature that concerns the application of conducting polymers as adsorbents of organic dyes and toxic heavy-metal ions.[6,7] This field also opens new perspectives for the ring-substituted derivatives of conducting polymers, *e.g.*, polyphenylenediamines,[8] that have been regarded so far to be of marginal importance due to their low conductivity.

The present study concerns the gradual conversion of polypyrrole to nitrogen-containing carbons and its impact on the adsorption of organic dyes. It is generally anticipated that the increase in the specific surface area of adsorbents would be of benefit to the adsorption capacity. The tuning of morphology represented by the preparation of one-dimensional morphologies, such as nanotubes or nanofibers, instead of globules, and reduction of their sizes is one of the approaches.[9,10] For that reason, three different polypyrrole morphologies, globules, nanofibers and nanotubes, have been compared in the present study.

Thermal treatment is another way to affect the surface area in conducting polymers at the expense of the changes in their

[a] *Institute of Macromolecular Chemistry, Academy of Sciences of the Czech Republic, 162 06 Prague 6, Czech Republic. E-mail: stejskal@imc.cas.cz*
[b] *University of Pardubice, Faculty of Chemical Technology, Pardubice 532 10, Czech Republic*
[c] *University of Chemistry and Technology Prague, Central Laboratories, 188 28 Prague 6, Czech Republic*
[d] *J. E. Purkyně University, Faculty of Science, 400 96 Ústí nad Labem, Czech Republic*
[e] *Charles University, Faculty of Mathematics and Physics, 180 00 Prague 8, Czech Republic*

molecular structure and conductivity.[11] When heating polypyrrole hydrochloride, the loss of acid associated with the deprotonation might have some effect on mesopore formation and increase the specific surface area. The specific surface area of globular polypyrrole increased from 75 $m^2 g^{-1}$ to 211 $m^2 g^{-1}$ after being exposed to 650 °C in an inert atmosphere.[12] The carbonization and activation at the same temperature produced carbon materials with a specific surface area exceeding 1000 $m^2 g^{-1}$.[13–15] The reported results are compared with those obtained in the present study.

Polypyrrole nanotubes are of special interest due to their uniform morphology.[10] They convert similarly to nitrogen-containing carbon nanotubes[12,16–20] and can be applied as new nanostructured nitrogen-enriched carbons. The carbonization of polypyrrole nanotubes improved the specific surface area from 86 $m^2 g^{-1}$ to 105 $m^2 g^{-1}$.[20] A specific surface area enhancement after carbonization,[21] *viz.* 205 $m^2 g^{-1}$[18] and 257 $m^2 g^{-1}$[16] has also been reported. The carbonized polypyrrole nanotubes offer an alternative to multiwalled carbon nanotubes from the morphological point of view but their structure and properties are different. They are suitable for energy-storage devices, such as electrochemical capacitors[22,23] or as electrocatalysts of oxygen reduction reaction,[24,25] and in the catalysis of organic transformations,[17] where the combination of conductivity and electroactivity with a high specific surface area is of benefit.

Polypyrrole has been studied as an adsorbent of rather universal character. Its applications as dye adsorbents or photocatalysts in dye decomposition have received the most attention[7] in addition to the removal of toxic chromium(VI),[26,27] heavy-metal ions,[6,28] drugs and cosmetics,[29] hydrocarbons[30] or influenza viruses.[31] Despite the expected activity of carbonized analogues of polypyrrole, nitrogen-containing carbons have received only marginal attention. For example, the adsorption capacity of alkali-activated carbonized polypyrrole for methyl orange was reported to exceed 500 mg g^{-1}.[32]

The present study merges the two research strategies outlined above: (1) the preparation of polypyrrole with a controlled nanostructure and (2) its gradual conversion to nitrogen-containing carbonaceous materials followed by testing in the adsorption of organic dye. Attention has especially been paid to the relation between the polypyrrole morphology and dye adsorption performance.

2. Experimental

2.1. Preparation

Three polypyrroles with different morphologies have been selected for the present study. Globular polypyrrole was prepared by the classic oxidation of 0.2 M pyrrole with 0.5 M iron(III) chloride in aqueous medium at room temperature (Fig. 1). Polypyrrole nanofibers were synthesized similarly using 0.2 M pyrrole and 0.2 M iron(III) chloride in the presence of 0.01 M Acid Blue 25 dye.[33] Finally, polypyrrole nanotubes originated in the oxidation of 0.05 M pyrrole with 0.05 M iron(III) chloride along with 0.0025 M methyl orange (Acid Orange 52).[9,10,34] Polypyrroles were obtained as intractable fluffy black powders that could be compressed to pellets for conductivity determination. All chemicals were of analytical grade supplied by Sigma Aldrich and used as delivered.

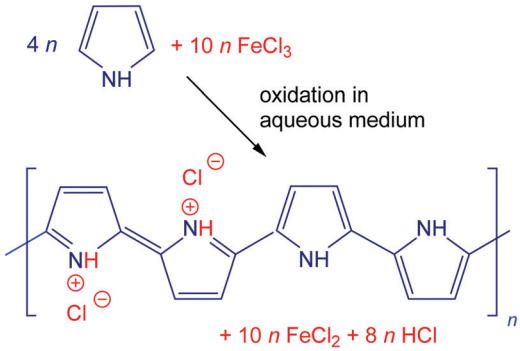

Fig. 1 The oxidation of pyrrole with iron(III) chloride to polypyrrole.

The preparative pyrolysis of polypyrrole was carried out with 1–2 g samples placed in quartz-glass containers and heated in a cylindrical furnace Clasic 10013T (Clasic CZ Ltd) under argon at the rate of 5 °C min^{-1} to the desired temperature. After reaching the target temperature, the power was switched off and the samples were left to cool still under an inert atmosphere.

2.2. Characterization

Morphology was observed using a scanning ultra-high-resolution electron microscope MAIA3 Tescan. Thermogravimetric analysis was carried out using a PerkinElmer Pyris 1 Thermogravimetric Analyzer in the temperature range 30–850 °C at a 5 °C min^{-1} rate and 20 mL min^{-1} nitrogen flow. Contents of carbon, hydrogen and nitrogen were determined using PerkinElmer 2400 Series II CHNS/O Analyzer.

Specific surface area and pore volume were determined from the adsorption and desorption isotherms on a NOVA3200 (Quantachrome Instruments) using NovaWin software. Samples were degassed for 24 h at 100 °C, then nitrogen adsorption and desorption isotherms were recorded (Linde, 99.999%). Five-point Brunauer–Emmett–Teller (BET) analysis has been applied for the total surface area determination and the 40-point Barrett–Joyner–Halenda (BJH) model for determining pore volume. Each sample was measured four times with an experimental error of 5%.

The conductivity was determined by the four-point van der Pauw method on pellets 13 mm in diameter and *ca.* 1 mm in thickness prepared at 527 MPa in a hydraulic press when such a preparation was feasible. The set-up used the current source Keithley 220, a Keithley 2010 multimeter and a Keithley 705 scanner with a Keithley 7052 matrix card. The powders have also been characterized using the van der Pauw method when compressed at 10 MPa in a lab-made cylindrical glass cell with an inner diameter of 10 mm between an insulating support and a glass piston carrying four platinum/rhodium electrodes on the perimeter of its base. The pressure was controlled using an L6E3 load cell (Zemic Europe BV, The Netherlands). The set-up for *in situ* resistivity determination was the same as that described above.

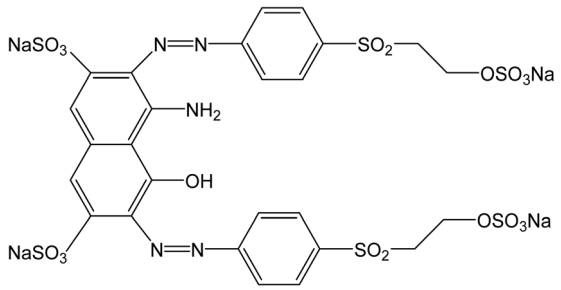

Fig. 2 Reactive Black 5.

The FTIR spectra of the powdered samples were analysed using a Nicolet 6700 spectrometer (Thermo-Nicolet, USA) equipped with reflective ATR extension GladiATR (PIKE Technologies, USA) with a diamond crystal. Spectra were recorded in the 4000–400 cm^{-1} region using a DLaTGS (deuterated L-alanine doped triglycine sulfate) detector at a resolution of 4 cm^{-1}, 64 scans and Happ–Genzel apodization.

2.3. Dye adsorption

The anionic dye, Reactive Black 5, has been selected as sorbate (Fig. 2). 50 mg portions of polypyrrole were suspended in 50 mL of the dye solution in water (100 mg L^{-1}) at room temperature and occasionally stirred gently. The dye/adsorbent mass ratio was 0.1. UV-vis spectra of the dye solution were recorded in relation to time in a 0.2 cm quartz cell using a PerkinElmer Lambda 20 UV-Vis spectrometer.

3. Results and discussion

3.1. Morphology

Polypyrrole can be prepared by the oxidation of pyrrole with iron(III) chloride in a variety of morphologies. The ordinary globular morphology transforms to one-dimensional nanofibers or nanotubes when the oxidation of pyrrole takes place in the presence of various organic dyes[35] (Fig. 3, left), such as methyl orange[10,17,36] or Acid Blue 25[33] used in the present study. The presence of a cavity inside the nanotubes[9,12] and its absence in nanofibers[33] has been earlier demonstrated by transmission electron microscopy. The individual polypyrrole morphologies differ in properties, and enhancement of conductivity and specific surface area is observed for one-dimensional types.[10]

It has been well established that the general features of morphology become preserved after carbonization except for some shrinkage[16,17,34] (Fig. 3, right). The gradual conversion of a conducting polymer to a nitrogen-containing carbon analogue and the associated changes in material properties were thus investigated in more detail.

3.2. Thermal treatment

Introductory thermogravimetric analysis revealed the conversion of polypyrrole to nitrogen-containing carbon at the analytical scale for all three polypyrrole samples differing in morphology (Fig. 4). Polypyrrole globules, nanofibers and nanotubes followed a similar pattern.

The preparative carbonization copies the trend observed in thermogravimetry and the residues left after the thermal exposure exceed 50 wt% (Fig. 5). The residues left at 650 °C were 50.6 wt% for globules, 61.5 wt% for nanofibers, and 60.8 wt% for nanotubes. The yield was sufficiently high to allow for the economic production of carbonized polypyrrole.

The scenario of the changes occurring in polypyrroles during thermal treatment is suggested to proceed as follows: (1) in the temperature region of 100–200 °C, the removal of residual humidity and starting of deprotonation take place (Fig. 6) when polypyrrole salts convert to corresponding bases by releasing hydrochloric acid[38,39] (Fig. 7). (2) This stage is followed by the gradual transformation of polypyrrole to nitrogen-containing carbon and the associated change in the molecular structure. (3) The next stage is the ripening of carbonized polypyrrole associated with continuing mass loss above 400 °C. This hypothesis is compared below with the elemental analysis and FTIR spectroscopy.

3.3. Composition

The changes in the elemental composition with temperature are illustrated only for the globular polypyrrole (Fig. 8) because, based on the residual masses (Fig. 5), they are expected to be the same for all three polypyrrole morphologies. The compositional trends are in accordance with the earlier analysis of the carbonization of polypyrrole nanotubes.[11,16]

The theoretical composition (wt%) calculated for the idealized segment of polypyrrole salt $C_{16}H_{12}N_4Cl_2$ (Fig. 7) is 58.01% C, 3.63% H, 16.92% N, 21.45% Cl, and similarly for the polypyrrole base $C_{16}H_{10}N_4$ it is 74.42% C, 3.88% H, 21.71% N. The content of all elements is lower than this expectation (Fig. 8), obviously due to the presence of other elements, such as oxygen or chlorine. The marked presence of oxygen atoms is rather puzzling. In principle, the presence of complex counter-ions $FeCl_4^-$ could account for the presence of other atoms. A small residue of $\approx$2 wt% found after thermogravimetric analysis in air,[12,20] however, does not favour this hypothesis. The inorganic residue in globular polypyrrole determined in the present case as ash was 2.62 wt%. Iron compounds thus cannot account for the presence of atoms other than C, H, and N.

The carbon content steadily increased as the exposure temperature increased (Fig. 8). This is mainly due to the deprotonation of polypyrrole salt which liberates hydrochloric acid (Fig. 7) and converts to a carbon-richer polypyrrole base. This trend continues above 400 °C due to the starting carbonization. The hydrogen content decreases both due to the deprotonation and subsequent carbonization, when single bonds are replaced by double ones.

The fraction of nitrogen passes through a maximum. Its relative participation increases at first as the hydrochloric acid is released from the polypyrrole salt, *i.e.* the atoms like chlorine leave (Fig. 8). Above 400 °C the nitrogen content is reduced in response to the decreasing C/N atomic ratio (Fig. 9), when the five-membered pyrrole containing four carbon atoms obviously converts to a six-membered graphitic-like structure. The nitrogen content nevertheless stands above 12 wt% and the carbonized products can be regarded as nitrogen-containing carbons.

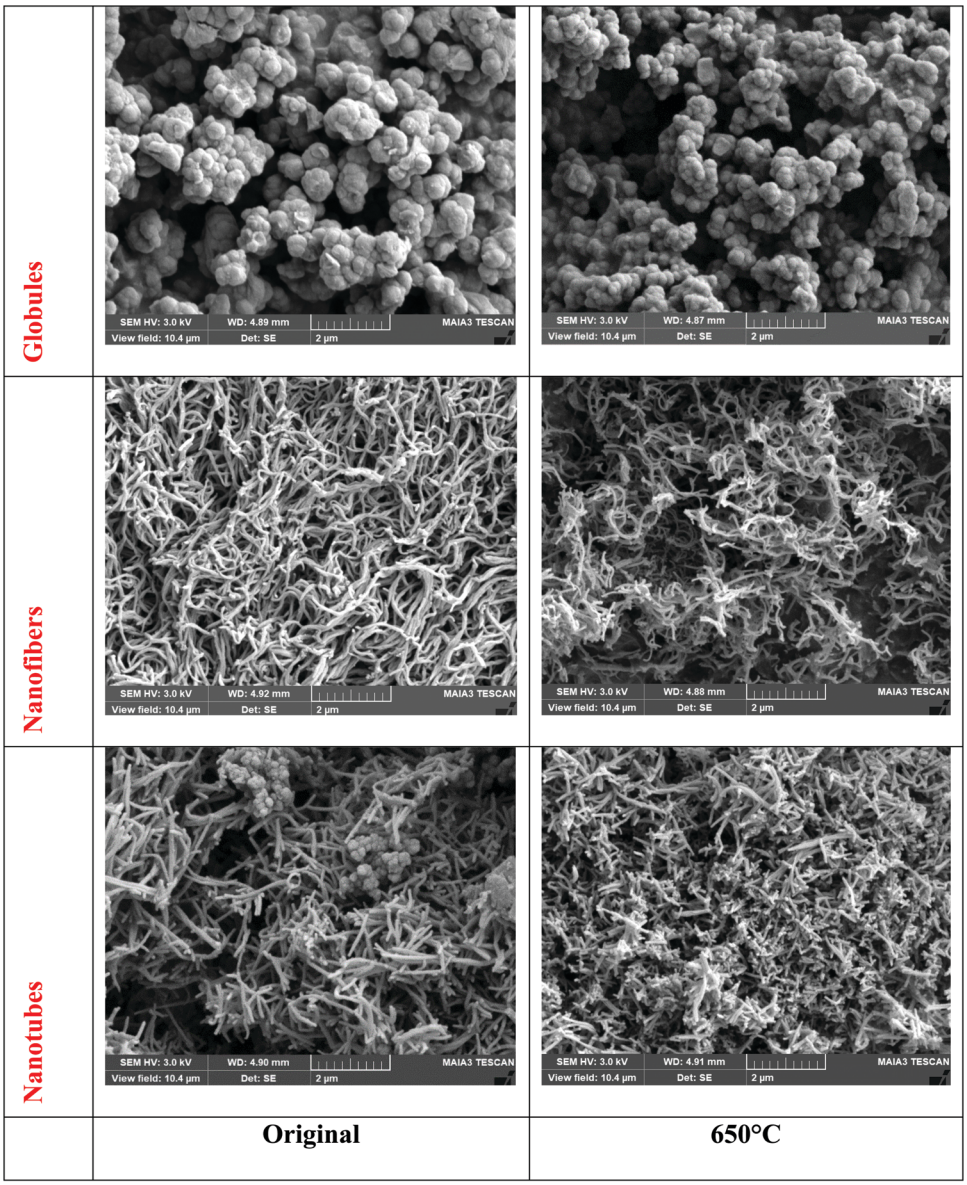

Fig. 3 Electron scanning micrographs of polypyrrole globules, nanofibers and nanotubes before (left) and after heating to 650 °C (right).

3.4. Specific surface area

Having in mind the application of conducting polymers and their carbonized analogues for the adsorption of organic dyes, the specific surface area is a parameter of interest. The specific surface area of the globular polypyrrole 12.4 $m^2\ g^{-1}$ is close to the values data reported in the literature, 10.6 $m^2\ g^{-1}$ [15] or 12.1 $m^2\ g^{-1}$.[40] The specific surface area of one-dimensional morphologies was higher as a rule[10] but still of the order of tens of $m^2\ g^{-1}$,[34,41,42] also in agreement with the present data on polypyrrole nanofibers and nanotubes (Table 1). The different specific surface areas are also demonstrated in adsorption/desorption isotherms (Fig. 10) for all original samples – globules, nanofibers and nanotubes.

The higher pore volume (Table 2) corresponds to the higher specific surface area, and increases from globules to nanotubes and nanofibers. The comparison of pore sizes and size distribution for original globules and nanofibers clearly demonstrates that nanofibers have larger pores in comparison with the globular sample (Fig. 11).

The exposure of polypyrrole nanostructures to 650 °C had no notable effect on the specific surface area (Table 1). This is in the contrast to the literature, which reports a marked increase in the specific surface area to hundreds of $m^2\ g^{-1}$ with increasing temperature.[16,18,43,44] Also, the pore volume was somewhat dependent on the processing temperature (Table 2). The effect of increasing surface area and pore volume is perhaps visible only for nanofibers and nanotubes, when pore volume increased after heating.

3.5. Conductivity

The conductivity is a basic parameter of polypyrrole studies. Conductivities of 0.23, 16.2, and 16.3 S cm^{-1} were found for

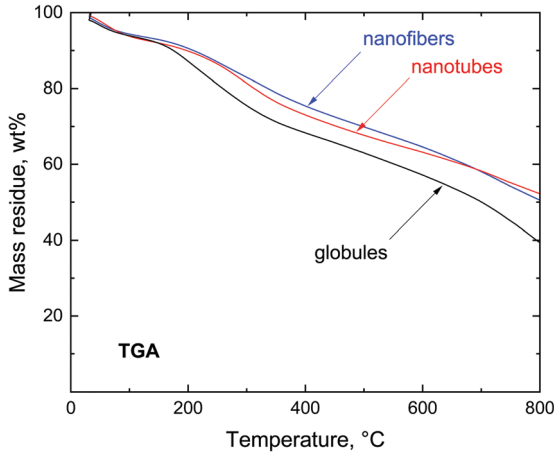

Fig. 4 Thermogravimetric analysis of polypyrroles in a nitrogen atmosphere.

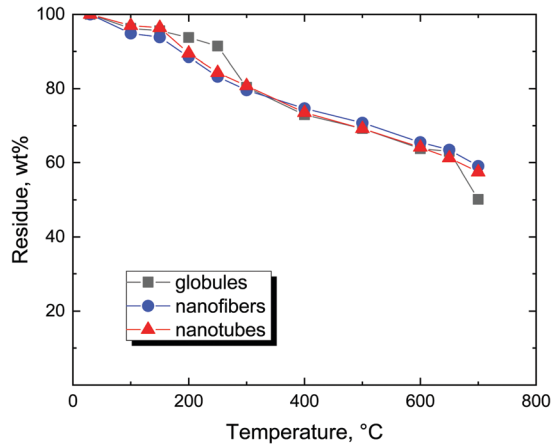

Fig. 5 Residual mass after preparative exposure of polypyrrole in argon to elevated temperatures.

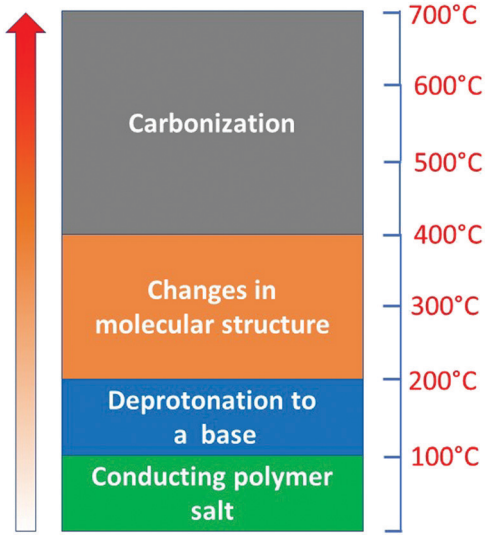

Fig. 6 Evolution of the molecular structure in polypyrrole exposed to elevated temperatures.

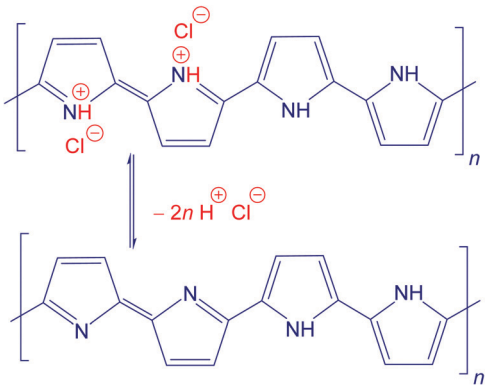

Fig. 7 Deprotonation: the conversion of polypyrrole salt to the corresponding base.

polypyrrole globules, nanotubes and nanofibers, respectively. After being exposed to elevated temperature, the conductivity of all three polypyrroles followed the same trend (Fig. 12). It gradually decreased at first with temperature increasing to 400 °C and levelled at the order of 10^{-4} S cm^{-1}. This is explained by gradual conversion of polypyrrole salt to a less conducting base.[38] The trend is reversed after 400 °C and most of the conductivity is recovered due to the carbonization, which generates new double bonds and converts polypyrrole to a conjugated graphitic structure.

Many polypyrrole samples exposed to elevated temperature could not be compressed to a pellet for the routine conductivity measurements. In such cases, the conductivity was determined by using a four-point van der Pauw method on the powder compressed to 10 MPa by a method specifically developed for this purpose (*cf.* Experimental). As expected, the conductivity values determined on powders were somewhat lower than those obtained with pellets compressed at 527 MPa but within the same order of magnitude (Fig. 12) and provided a good estimate of the material conductivity.

3.6. FTIR spectra

Vibrational spectroscopy is a potent tool to identify and describe the changes at the molecular level. The deprotonation of polypyrrole and its starting decomposition processes outlined above can be conveniently followed by FTIR spectroscopy (Fig. 13). The different morphologies of the initial polypyrrole globules, nanofibers and nanotubes are reflected in their infrared spectra.[10] The polaron band above 1700 cm^{-1} characteristic for conducting polymers is more pronounced in the spectra of nanofibers and nanotubes. This correlates well with their higher conductivity. The main band of globular polypyrrole situated at 1536 cm^{-1} (C–C stretching vibrations in the pyrrole ring) is shifted to 1518 cm^{-1} in the spectra of nanofibers and nanotubes. The starting deprotonation is characterized mainly by the decreasing polaron band and by its shift to 1553 cm^{-1} in the spectrum of globular polypyrrole and to 1548 cm^{-1} in the spectra of nanofibres and nanotubes. This happens at 300 °C for globules, at 150 °C for nanofibers and at 200 °C for nanotubes. The deprotonation is reflected also in the shifts of other bands in

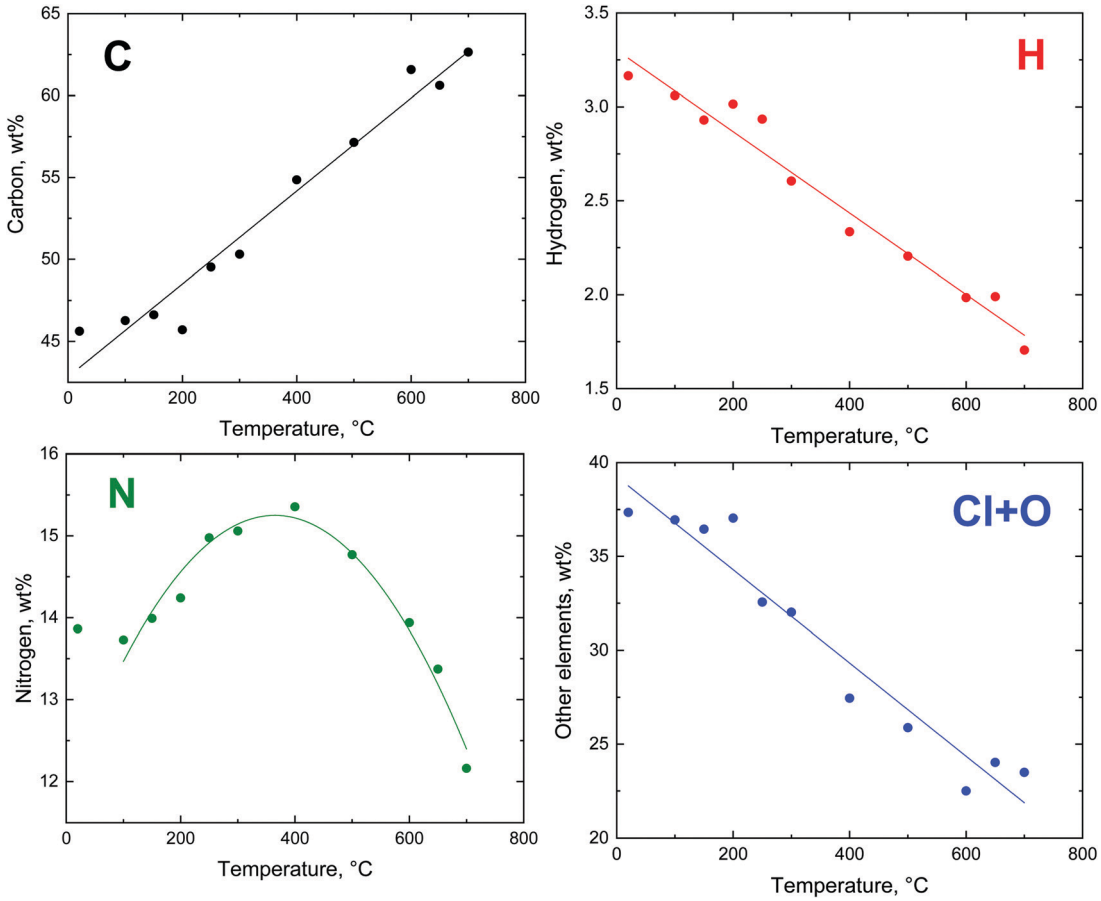

Fig. 8 The trends in the evolution of elemental composition after the exposure of globular polypyrrole to elevated temperature.

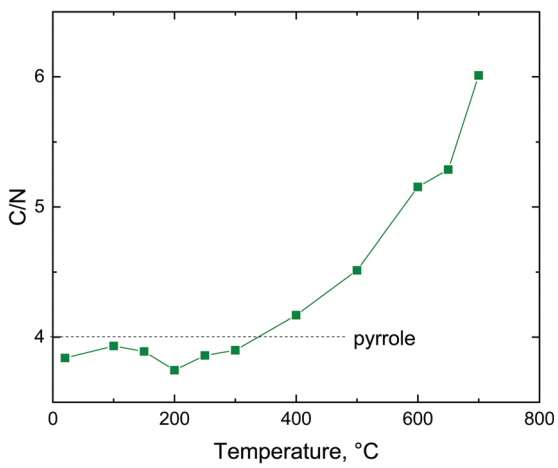

Fig. 9 The carbon/nitrogen atomic ratio in polypyrrole after heating to various temperatures.

Table 1 Specific surface area (in m^2 g^{-1}) of polypyrroles exposed to various temperatures

Morphology	20 °C	200 °C	400 °C	650 °C
Globules	12.4 ± 0.2	13.0 ± 1.2	21.5 ± 4.4	12.6 ± 0.4
Nanofibers	65.1 ± 2.1	68.6 ± 1.5	71.0 ± 8.7	87.0 ± 3.7
Nanotubes	45.2 ± 8.8	48.0 ± 7.0	58.3 ± 2.7	55.9 ± 0.6

the infrared spectra: the band with the maximum at 1438 cm^{-1} (C–N stretching vibrations in the ring) in the spectrum of globules shifts to 1467 cm^{-1}, and from 1425 and 1439 cm^{-1} to 1462 and 1468 cm^{-1} for nanofibers and nanotubes, respectively. The band with a maximum at 1287 cm^{-1} (C–H and C–N in-plane deformation modes) in the spectrum of globules remains at this position, but shifts from 1271 to 1298 cm^{-1} and from 1278 to 1293 cm^{-1} for nanofibers and nanotubes, respectively. The band situated at 1149 cm^{-1} (breathing vibrations of the pyrrole ring) in the spectrum of globules shifts to 1178 cm^{-1}, and shifts from 1123 to 1170 cm^{-1} and from 1120 to 1170 cm^{-1} in the spectra of nanofibers and nanotubes. The deprotonation also manifests itself by the relative decrease in the ratio of the intensity of the peak situated at 1001 cm^{-1} (C–H out-of-plane deformation vibrations of the ring) to that at 1041 cm^{-1} (C–H and C–N in-plane deformation vibrations) in the spectrum of globules, and of 990 to 1029 cm^{-1} for nanofibers, and of 993 to 1028 cm^{-1} for nanotubes. The described changes in the infrared spectra of polypyrrole globules, nanofibers and nanotubes after heating in this region of temperatures correspond well to the changes observed in the spectra of polypyrrole after deprotonation using

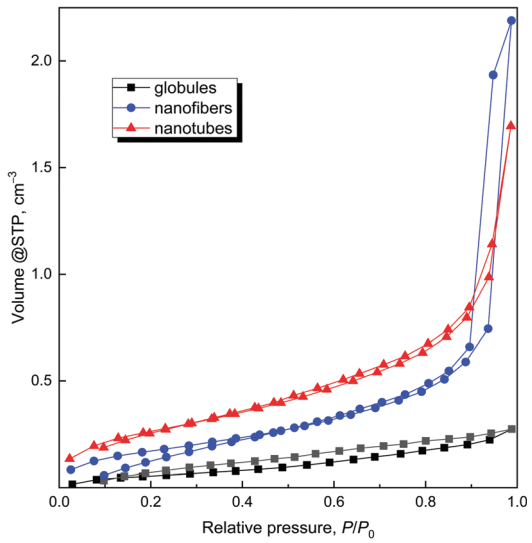

Fig. 10 Adsorption/desorption isotherms of original polypyrroles.

Table 2 Pore volume (in cm^3 g^{-1}) of polypyrroles exposed to various temperatures

Morphology	20 °C	200 °C	400 °C	650 °C
Globules	0.060 ± 0.004	0.035 ± 0.001	0.046 ± 0.005	0.034 ± 0.004
Nanofibers	0.240 ± 0.077	0.224 ± 0.038	0.258 ± 0.125	0.290 ± 0.001
Nanotubes	0.135 ± 0.031	0.165 ± 0.009	0.174 ± 0.007	0.177 ± 0.007

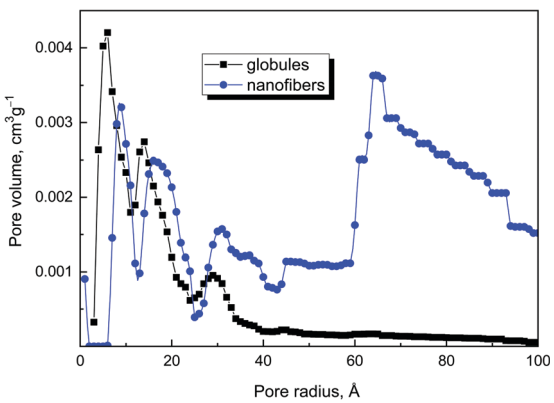

Fig. 11 Pore size distribution of original globules and nanofibers.

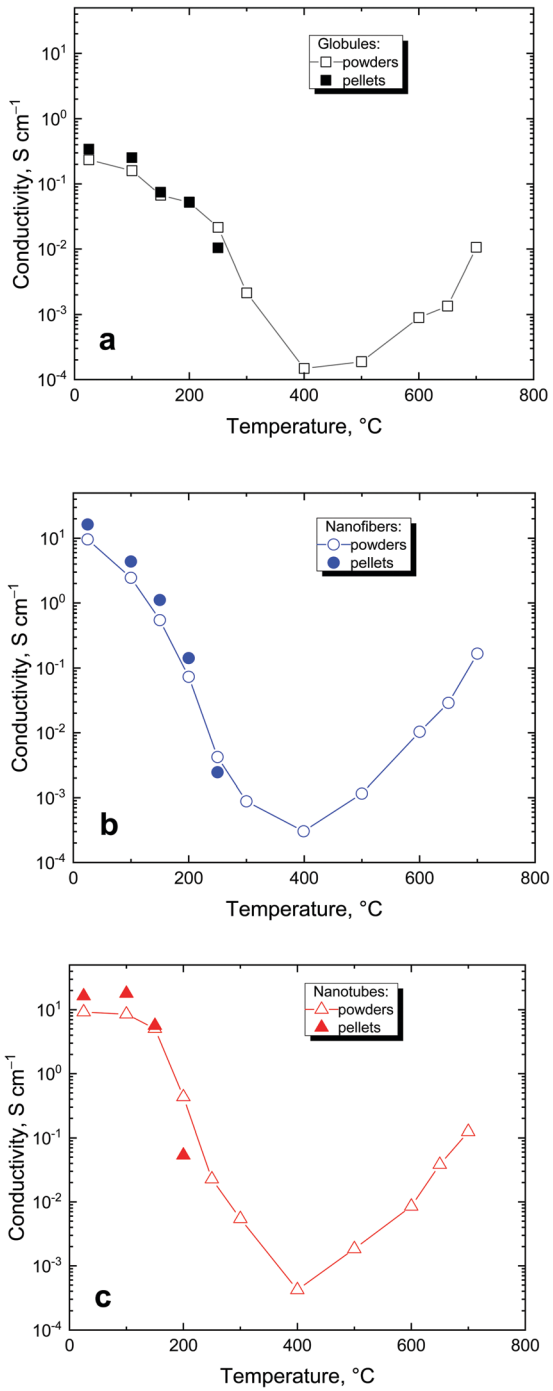

Fig. 12 The conductivity of polypyrrole powders determined after exposure to specific temperature under 10 MPa compression (open symbols) and of corresponding pellets prepared at 527 MPa: (a) globules, (b) nanofibers, (c) nanotubes.

1 M ammonium hydroxide.[38] The transformation of polypyrrole to carbon-like materials has been observed after heating above 400 °C for all morphologies: globules, nanofibers and nanotubes. This is demonstrated by the presence of two broad bands with maxima at 1553 and 1178 cm^{-1} in the spectrum of globular polypyrrole, at 1570 and 1150 cm^{-1} for nanofibers, and at 1565 and 1128 cm^{-1} in the spectrum of nanotubes.[37] The first one emerged from C–C stretching vibrations in the pyrrole ring and the second one from breathing vibrations of the pyrrole ring. They are characteristic of the Raman spectra of carbon-like materials (G- and D-bands)[16,45] and they are inactive in the FTIR spectra. In disordered samples, however, they become IR-active because of symmetry-breaking of the carbon network and the presence of the nitrogen atom in the structure.

4. Application

Conducting polymers may be applied in various directions not always exploiting the conductivity.[3] For example, it has been

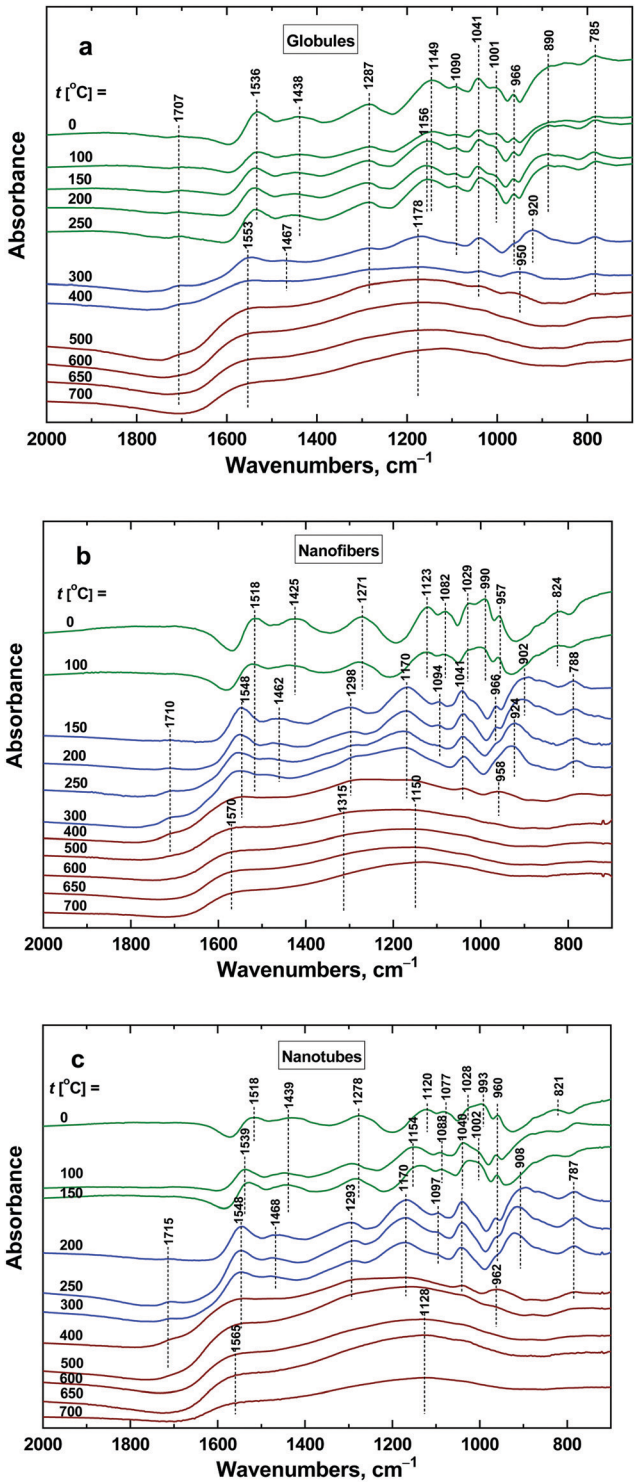

Fig. 13 ATR FTIR spectra of polypyrrole (a) globules, (b) nanofibers, and (c) nanotubes exposed to various temperatures.

demonstrated in a number of papers that conducting polymers can efficiently adsorb organic dyes or stimulate their photocatalytic decomposition[7] and thus be considered in environmental issues, such as water-pollution treatment. It was the purpose of this study to discuss factors that might affect or control the adsorption of organic dyes on polypyrrole and its heat-treated analogues. They are represented by electrostatic ionic and π–π interactions, hydrogen bonding, and hydrophobic or dispersion forces of the van der Waals type. It is believed that the observed interaction between conducting polymers and dyes is due to π–π interactions in the conjugated structure that both moieties share. Polypyrrole is a polycation but as it adsorbs well both the anionic and cationic dyes,[7] the electrostatic interactions are therefore believed not to be operational. Other types of interactions are expected to be of secondary importance. An anionic dye, Reactive Black 5 (Fig. 2), has been selected as an example for the adsorption feasibility study. The authors are aware that the results for other dyes, under various acidity conditions, and concentrations of a dye and an adsorbent might provide different results.

4.1. Original polypyrroles

The changes in the dye concentration due to the adsorption on conducting polymers can be followed by UV-vis spectroscopy, when the relative decrease of the dye is proportional to the corresponding optical absorbance at local maxima as follows from the Lambert–Beer law (Fig. 14). Over 95% of dye was removed from the aqueous medium by polypyrrole nanofibers within the allocated time of several days (Fig. 14 and 15). This means that the adsorption capacity of polypyrrole nanofibers was at least close to 100 mg g^{-1}.

The course of the dye adsorption can be also expressed as a residual fraction C/C_0 of the original dye concentration C_0 (Fig. 16), which is directly linked to the decrease in the corresponding optical absorbance. It is obvious that globular polypyrrole is the least efficient of the three morphologies, and nanotubes approach the performance of nanofibers that perform the best. The correlation with the specific surface area and pore volume of polypyrrole is obvious. The adsorption efficiency order, from globules to nanotubes and nanofibers, is maintained also for the polypyrroles treated at elevated temperature (Fig. 16), indicating that the specific surface area is always one of the parameters controlling the adsorption.

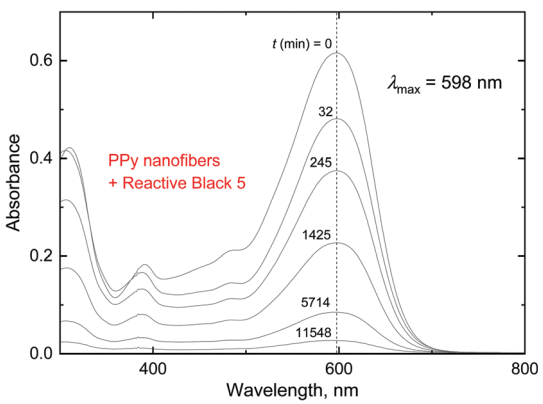

Fig. 14 The decrease in the optical absorbance of the Reactive Black 5 solution with time, t. 5 mg of Reactive Black 5 and 50 mg of polypyrrole nanofibers in 50 mL of water; 20 °C.

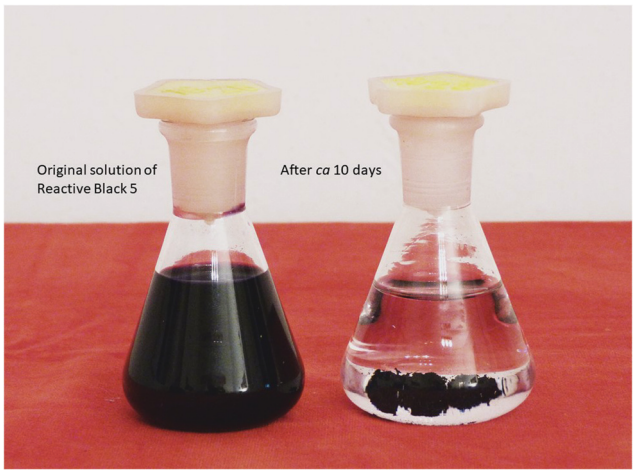

Fig. 15 The solution of Reactive Black 5 before (left) and after adsorption of the dye by polypyrrole nanofibers (right).

4.2. After treatment at 100–250 °C

The adsorption efficiency of polypyrrole treated at 200 °C is significantly lower (Fig. 16). The polypyrrole polycation is converted at least partly to a neutral polypyrrole base, as confirmed by the conductivity decrease (Fig. 12) and FTIR spectra (Fig. 13). Ionic interactions can be ruled out after the deprotonation of polypyrrole but they are not believed to be responsible even in the protonated form. It is rather the higher hydrophobicity of the polypyrrole base compared with that of the original polypyrrole salt that affects the interaction between the conducting polymer and a dye.

4.3. Above 400 °C

After treatment of the polypyrroles above 400 °C, the number of potential interactions is likely to be lower due to the reduced number of π–π interactions as the molecular structure of polypyrrole becomes disordered. As a result, the material's ability to adsorb a dye decreases (Fig. 16). The hydrogen bonding, *e.g.*, between amino groups in dyes and the nitrogen atom still incorporated in the carbonized structure would be still possible. Please note that the ratio C/C_0 formally exceeds unity (Fig. 16). This is due to the dispersion of fine non-sedimenting carbonized particles that create a grey background shifting the dye spectrum to higher absorbances.

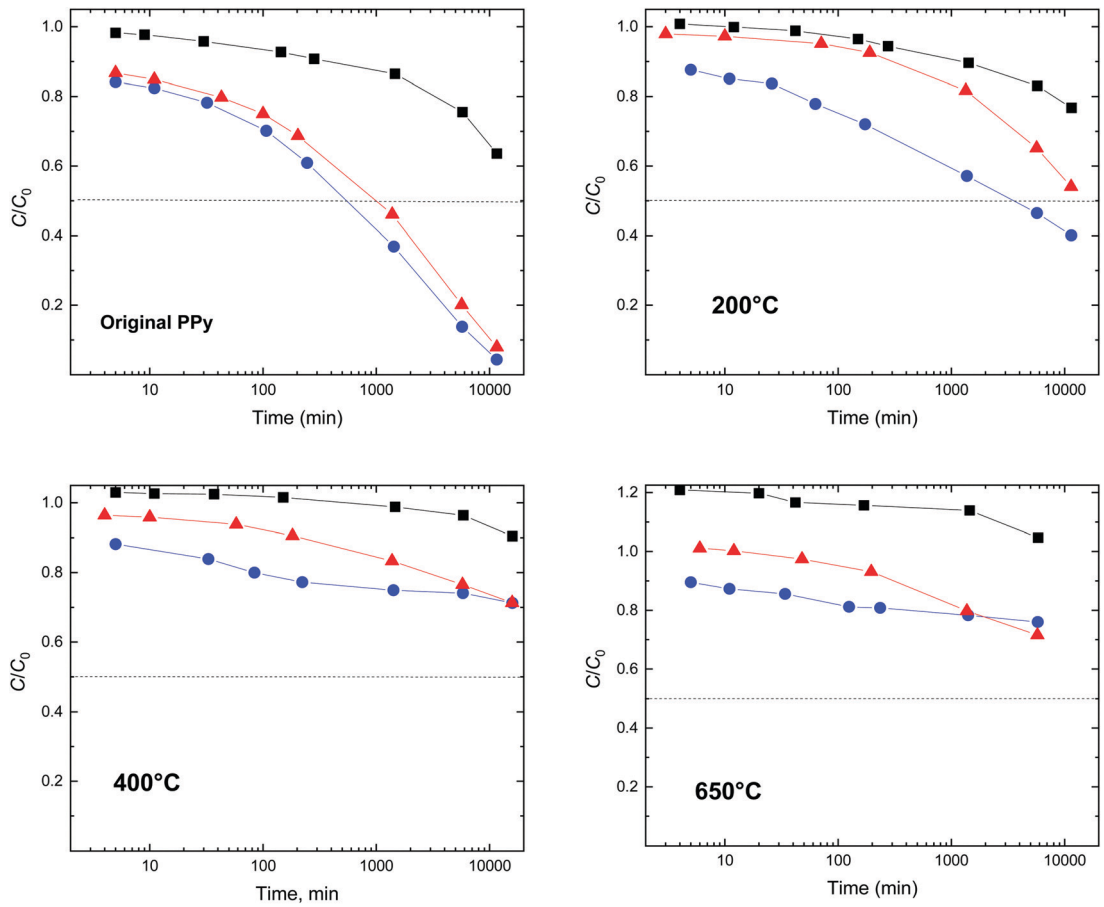

Fig. 16 Relative decrease in the concentration of Reactive Black 5, C/C_0, in the presence of globular polypyrrole (black squares), polypyrrole nanotubes (red triangles) and nanofibers (blue circles) dispersed in water. Polypyrroles were exposed to 200, 400 or 650 °C prior to the dye adsorption test. Original dye concentration C_0 = 100 mg L^{-1}, polypyrrole adsorbent: 1 g L^{-1}, 20 °C.

5. Conclusions

The objective of the manuscript was (1) to study the gradual conversion of conducting polypyrrole to nitrogen-enriched carbon, (2) to compare the behaviour of individual morphologies (globules, nanotubes, and nanofibers), and (3) to illustrate one of the potential applications of prepared materials, organic dye adsorption. The important conclusions with respect to conductivity are (a) the conductivity differs substantially for the individual polypyrrole morphologies and (b) it decreases with temperature of exposure at first but nearly recovers at higher temperatures. With respect to organic dye adsorption we found that (a) its extent strongly depended on the polypyrrole morphology; nanofibers and nanotubes were good adsorbents but the performance of globular polypyrrole was marginal. Finally, (b) the dye adsorption efficiency was reduced as the conducting polymer converted to the corresponding carbon material.

For the potential application of conducting polymers in water-pollution treatment, the increase in their specific surface areas by morphology tuning is a primary goal. Electroactivity of conducting polymers may provide an added value that enables the control of adsorption properties by applied electrical potential.[46] In addition, ring-substituted conducting polymers, *e.g.*, polyphenylenediamines,[8] have been of limited interest due to their low conductivity. They may become, however, prospective materials for the environmental studies aimed at the removal of organic pollutants.

Conflicts of interest

The authors declare no conflict of interest.

Acknowledgements

The authors thank the Czech Science Foundation for the financial support (19-04859S).

References

1 J. Stejskal and R. G. Gilbert, Polyaniline. Preparation of a conducting polymer (IUPAC technical report), *Pure Appl. Chem.*, 2002, **74**, 857–867, DOI: 10.1351/pac200274050857.
2 F. Kazemi, S. M. Naghib and Z. Mohammadpour, Multifunctional micro-nanoscaled structures based on polyaniline: an overview of modern emerging devices, *Mater. Today Chem.*, 2020, **16**, 100249, DOI: 10.1016/j.mtchem.2020.100249.
3 J. Stejskal, Conducting polymers are not just conducting: a perspective for emerging technology, *Polym. Int.*, 2020, **69**, 662–664, DOI: 10.1002/pi.5947.
4 P. Humpolíček, V. Kašpárková, J. Pachernik, J. Stejskal, P. Bober, Z. Capáková, K. A. Radaszkiewicz, I. Junkar and M. Lehocký, The biocompatibility of polyaniline and polypyrrole: a comparative study of their cytotoxicity, embryotoxicity and impurity profile, *Mater. Sci. Eng., C*, 2018, **91**, 303–310, DOI: 10.1016/j.msec.2018.05.037.
5 K. Parashar, D. Prajapati, R. McIntyre and B. Kandasubramanian, Advancements in biological neural interfaces using conducting polymers: a review, *Ind. Eng. Chem.*, 2020, **59**, 9707–9718, DOI: 10.1021/acs.iecr.0c00174.
6 M. L. Sall, A. K. D. Diaw, D. Gningue-Sall, S. E. Aaron and J. J. Aaron, Toxic heavy metals: impact on the environment and human health, and treatment with conducting organic polymers, a review, *Environ. Sci. Pollut. Res.*, 2020, **27**, 29927–29942, DOI: 10.1007/s11356-020-09354-3.
7 J. Stejskal, Interaction of conducting polymers, polyaniline and polypyrrole, with organic dyes: polymer morphology control, dye adsorption and photocatalytic decomposition, *Chem. Pap.*, 2020, **74**, 1–54, DOI: 10.1007/s11696-019-00982-9.
8 J. Stejskal, Polymers of phenylenediamines, *Prog. Polym. Sci.*, 2015, **41**, 1–31, DOI: 10.1016/j.progpolymsci.2014.10.007.
9 I. Sapurina, Y. Li, E. Alekseeva, P. Bober, M. Trchová, Z. Morávková and J. Stejskal, Polypyrrole nanotubes: the tuning of morphology and conductivity, *Polymer*, 2017, **113**, 247–258, DOI: 10.1016/j.polymer.2017.02.064.
10 J. Stejskal and M. Trchová, Conducting polypyrrole nanotubes: a review, *Chem. Pap.*, 2018, **72**, 1563–1595, DOI: 10.1007/s11696-018-0394-x.
11 G. Ćirić-Marjanović, I. Pašti, N. Gavrilov, A. Janosević and S. Mentus, Carbonised polyaniline and polypyrrole: towards advanced nitrogen-containing carbon materials, *Chem. Pap.*, 2013, **67**, 781–813, DOI: 10.2478/s11696-013-0312-1.
12 J. Kopecká, M. Mrlík, R. Olejník, D. Kopecký, M. Vrňata, J. Prokeš, P. Bober, Z. Morávková, M. Trchová and J. Stejskal, Polypyrrole nanotubes and their carbonized analogs: synthesis, characterization, gas sensing properties, *Sensors*, 2016, **16**, 1917, DOI: 10.3390/s16111917.
13 M. Sevilla, R. Mokaya and A. B. Fuertes, Ultrahigh surface area polypyrrole-based carbons with superior performance for hydrogen storage, *Energy Environ. Sci.*, 2011, **4**, 2930–2936, DOI: 10.1039/c1ee01608c.
14 L. Qie, W. M. Chen, Z. H. Wang, Q. G. Shao, X. Li, L. X. Yuan, X. L. Hu, W. X. Zhang and Y. H. Huang, Nitrogen-doped porous carbon nanofiber webs as anodes for lithium ion batteries with a superhigh capacity and rate capability, *Adv. Mater.*, 2012, **24**, 2047–2050, DOI: 10.1002/adma.201104634.
15 Z. Wang, N. Goyal, L. Y. Liu, D. C. W. Tsang, J. Shang, W. J. Liu and G. Li, N-doped porous carbon derived from polypyrrole for CO_2 capture from humid flue gases, *Chem. Eng. Sci.*, 2020, **396**, 125376, DOI: 10.1016/j.cej.2020.125376.
16 G. Ćirić-Marjanović, S. Mentus, I. Pašti, N. Gavrilov, J. Krstić, J. Travas-Sejdic, L. T. Strover, J. Kopecká, Z. Morávková, M. Trchová and J. Stejskal, Synthesis, characterization, and electrochemistry of nanotubular polypyrrole and polypyrrole-derived carbon nanotubes, *J. Phys. Chem. C*, 2014, **118**, 14770–14784, DOI: 10.1021/jp502862d.
17 I. Sapurina, J. Stejskal, I. Šeděnková, M. Trchová, J. Kovářová, J. Hromádková, J. Kopecká, M. Cieslar, A. Abu El-Nasr and M. M. Ayad, Catalytic activity of polypyrrole nanotubes decorated with noble-metal nanoparticles and their conversion to carbonized analogues, *Synth. Met.*, 2016, **214**, 14–22, DOI: 10.1016/j.synthmet.2016.01.009.

18 M. C. Wu, T. S. Zhao, R. H. Zhang, L. Wei and H. R. Jiang, Carbonized tubular polypyrrole with a high activity for the Br_2/Br^- redox reaction in zinc-bromine flow batteries, *Electrochim. Acta*, 2018, **284**, 569–576, DOI: 10.1016/j.electacta.2018.07.192.

19 Z. P. Kang, Y. H. P. J. Zhang and Z. G. Zhu, A shriveled rectangular carbon tube with the concave surface for high-performance enzymatic glucose/O_2 biofuel cells, *Biosens. Bioelectron.*, 2019, **132**, 76–83, DOI: 10.1016/j.bios.2019.02.044.

20 I. M. Minisy, N. Gavrilov, U. Acharya, Z. Morávková, C. Unterweger, M. Mičušík, S. K. Filippov, J. Kredatusová, I. A. Pašti, S. Breitenbach, G. Ćirić-Marjanović, J. Stejskal and P. Bober, Tailoring of carbonized polypyrrole nanotubes core by different polypyrrole shells for oxygen reduction reaction selectivity modification, *J. Colloid Interface Sci.*, 2019, **551**, 184–194, DOI: 10.1016/j.jcis.2019.04.064.

21 J. Lin, X. L. Xu, J. Wang, B. F. Zhang, D. Li, C. Wang, Y. L. Jin and J. B. Zhu, Nitrogen-doped hierarchically porous carbonaceous nanotubes for lithium ion batteries, *Chem. Eng. J.*, 2018, **352**, 964–971, DOI: 10.1016/j.cej.2018.06.057.

22 P. Bober, J. Pfleger, I. A. Pašti, N. Gavrilov, S. K. Filippov, D. Klepac, M. Trchová, H. Hlídková and J. Stejskal, Carbogels: carbonized conducting polyaniline/poly(vinyl alcohol) aerogels derived from cryogels for electrochemical capacitors, *J. Mater. Chem. A*, 2019, **7**, 1785–1796, DOI: 10.1039/c8ta09574d.

23 H. Q. Gao, D. Zhang, H. T. Zhou, J. C. Wu, C. Liu and G. J. Xu, Polypyrrole derived porous carbon for high-performance Li ion capacitors, *Vacuum*, 2020, **177**, 109360, DOI: 10.1016/j.vacuum.2020.109360.

24 C. Zhang, B. Ma and Y. K. Zhou, Three-dimensional polypyrrole derived *N*-doped carbon nanotube aerogel as a high-performance metal-free catalyst for oxygen reduction reaction, *ChemCatChem*, 2019, **11**, 5495–5504, DOI: 10.1002/cctc.201901334.

25 M. G. Wang, Y. N. Li and J. Han, Mesoporous N-doped carbon nanofibers with surface nanocavities for enhanced catalytic activity towards oxygen reduction reaction, *J. Mater. Sci.*, 2020, **55**, 11177–11187, DOI: 10.1007/s10853-020-04772-7.

26 S. Rafiaee, M. R. Samani and D. Toghraie, Removal of hexavalent chromium from aqueous media using pomegranate peels modified by polymeric coatings: effects of various composite synthesis parameters, *Synth. Met.*, 2020, **265**, 116416, DOI: 10.1016/j.synthmet.2020.116416.

27 S. Zaghlol, W. A. Amer, M. H. Shaaban, M. M. Ayad, P. Bober and J. Stejskal, Conducting macroporous polyaniline/poly(vinyl alcohol) aerogels for the removal of chromium(VI) from aqueous media, *Chem. Pap.*, 2020, **74**, 3183–3193, DOI: 10.1007/s11696-020-01151-z.

28 H. N. M. E. Mahmud, A. K. O. Huq and R. B. Yahya, The removal of heavy metal ions from wastewater/aqueous solution using polypyrrole-based adsorbents: a review, *RSC Adv.*, 2016, **6**, 14778–14791, DOI: 10.1039/c5ra24358k.

29 D. K. Yoo, H. J. An, H. A. Khan, G. T. Hwang and S. H. Jhung, Record-high adsorption capacities of polyaniline derived porous carbons for the removal of personal care products from water, *Chem. Eng. J.*, 2018, **352**, 71–78, DOI: 10.1016/j.cej.2018.06.144.

30 C. Della Pina, M. A. De Gregorio, P. Dellavedova and E. Falletta, Polyanilines as new sorbents for hydrocarbons removal from aqueous solutions, *Materials*, 2020, **13**, 2161, DOI: 10.3390/ma13092161.

31 V. T. Ivanova, E. O. Garina, E. I. Burtseva, E. S. Kirillova, M. V. Ivanova, J. Stejskal and I. Y. Sapurina, Conducting polymers as sorbents of influenza viruses, *Chem. Pap.*, 2017, **71**, 495–503, DOI: 10.1007/s11696-016-0068-5.

32 A. A. Alghamdi, A. B. Al-Odayni, W. S. Saeed, M. S. Almutairi, F. A. Alharthi, T. Aouak and A. Al-Kahtani, Adsorption of azo dye methyl orange from aqueous solutions using alkali-activated polypyrrole-based graphene oxide, *Molecules*, 2019, **24**, 3685, DOI: 10.2290/molecules24203685.

33 P. Bober, Y. Li, U. Acharya, Y. Panthi, J. Pfleger, P. Humpolíček, M. Trchová and J. Stejskal, Acid Blue dyes in polypyrrole synthesis: the control of polymer morphology at nanoscale in the promotion of high conductivity and the reduction of cytotoxicity, *Synth. Met.*, 2018, **237**, 40–49, DOI: 10.1016/j.synthmet.2018.01.010.

34 Y. Li, P. Bober, M. Trchová and J. Stejskal, Polypyrrole prepared in the presence of methyl orange and ethyl orange: nanotubes versus globules in the conductivity enhancement, *J. Mater. Chem. C*, 2017, **5**, 4236–4245, DOI: 10.1039/c7tc00206h.

35 J. Stejskal and J. Prokeš, Conductivity and morphology of polyaniline and polypyrrole prepared in the presence of organic dyes, *Synth. Met.*, 2020, **264**, 116373, DOI: 10.1016/j.synthmet.2020.116373.

36 X. M. Yang, Z. X. Zhu, T. Y. Dai and Y. Lu, Facile fabrication of functional polypyrrole nanotubes via a reactive self-degraded template, *Macromol. Rapid Commun.*, 2005, **26**, 1736–1740, DOI: 10.1002/marc.200500514.

37 M. Trchová, E. N. Konyushenko, J. Stejskal, J. Kovářová and G. Ćirić-Marjanović, The conversion of polyaniline nanotubes to nitrogen-containing carbon nanotubes and their comparison with multi-walled carbon nanotubes, *Polym. Degrad. Stab.*, 2009, **94**, 929–938, DOI: 10.1016/j.polymdegradstab.2009.03.001.

38 J. Stejskal, M. Trchová, P. Bober, Z. Morávková, D. Kopecký, M. Vrňata, J. Prokeš, M. Varga and E. Watzlová, Polypyrrole salts and bases: superior conductivity of nanotubes and their stability towards the loss of conductivity by deprotonation, *RSC Adv.*, 2016, **6**, 88382–88391, DOI: 10.1039/c6ra19461c.

39 J. Prokeš, M. Varga, M. Vrňata, S. Valtera and J. Stejskal, Nanotubular polypyrrole: reversibility of protonation/deprotonation cycles and long-term stability, *Eur. Polym. J.*, 2019, **115**, 290–297, DOI: 10.1016/j.eurpolymj.2019.03.037.

40 M. Tanzifi, M. T. Yaraki, Z. Beiramzadeh, L. H. Saremi, M. Najafifard, H. Moradi, M. Mansouri, M. Karami and H. Bazgir, Carboxymethyl cellulose improved adsorption capacity of polypyrrole/CMC composite nanoparticles for removal of reactive dyes: experimental optimization and DFT calculation, *Chemosphere*, 2020, **255**, 127052, DOI: 10.1016/j.chemosphere.2020.127052.

41 G. Q. Ma, Z. Y. Wen, Q. S. Wang, C. Shen, P. Peng, J. Jin and X. W. Wu, Enhanced performance of lithium sulfur battery with self-assembly polypyrrole nanotube film as the functional interlayer, *J. Power Sources*, 2015, **273**, 511–516, DOI: 10.1016/j.jpowsour.2014.09.141.

42 D. Kopecký, M. Varga, J. Prokeš, M. Vrňata, M. Trchová, J. Kopecká and M. Václavík, Optimization routes for high electrical conductivity of polypyrrole nanotubes prepared in the presence of methyl orange, *Synth. Met.*, 2017, **230**, 89–96, DOI: 10.1016/j.synthmet.2017.06.004.

43 Z. F. Zhou, Z. H. Zhang, H. R. Peng, Y. Qin, G. C. Li and K. Z. Chen, Nitrogen- and oxygen-containing activate carbon nanotubes with improved capacitive properties, *RSC Adv.*, 2014, **4**, 5524–5530, DOI: 10.1039/c3ra45076g.

44 Z. Y. Sui, X. Li, Z. Y. Sun, H. C. Tao, P. Y. Zhang and L. Zhao, Nitrogen-doped and nanostructured carbons with high surface area for enhanced oxygen reduction reaction, *Carbon*, 2018, **126**, 111–118, DOI: 10.1016/j.carbon.2017.10.003.

45 M. S. Dresselhaus, A. Jorio, M. Hofman, G. Dresselhaus and R. Saito, Perspectives on carbon nanotubes and graphene Raman spectroscopy, *Nano Lett.*, 2010, **10**, 751–758, DOI: 10.1021/nl904286r.

46 M. M. Haque and D. K. Y. Wong, Improved dye entrapment-liberation performance at electrochemically synthesized polypyrrole-reduced graphene oxide nanocomposite films, *J. Appl. Electrochem.*, 2017, **47**, 777–788, DOI: 10.1007/s10800-017-1079-9.